Supporting information

Electrostatic Asymmetry in the Reaction Center of Photosystem II

Frank Müh, Melanie Plöckinger, and Thomas Renger*

Institute of Theoretical Physics, Department of Theoretical Biophysics, Johannes Kepler University Linz, Altenberger Strasse 69, AT-4040 Linz, Austria

Corresponding Author

*E-mail: frank.mueh@jku.at. Phone: +43 (0)732 24685157.

Contents

Table index

Figure index

S1: Protein structure and electrostatic modeling

The calculations are based on the most recent refinements of crystal structures of cyanobacterial PSIIcc. These are the structure at 1.9 Å resolution by Umena et al.[1] for *T. vulcanus* (PDB 3WU2 superseding 3ARC) and the structure at 2.44 Å resolution by Hellmich et al.[2] for *T. elongatus* (PDB 4PJ0). Structural elements contained in the used models are collected in Tables S1 and S2, respectively.

Table S1: Structural elements contained in the full RC model based on PDB 3WU2 (*T. vulcanus*).

Peptide	Modeled amino acids	Patches [a]	Pigments and organic cofactors	Explicit water molecules
PsbA	Ala A11 – Ala A344	ACE,[b] NONE [c]	OEX A401, FE A402, CL A403, A404, CLA A 405 – A407, PHO A408, A409, CLA A410, BCR A411, SQD A412, LMG A413, PL9 414, SQD A418	A510, A513, A552, A563, A565
PsbD	Ala D12 – Leu D352	ACE,[b] NONE [c]	BCT D401, CLA D 402, D403, BCR D404, PL9 D405, SQD D407, LHG D408 – D410, LMG D411	D544
PsbE	Thr E4 – Lys E84	ACE,[b] CT3 [d]	LHG E101, DGD H102, LHG L101	–
PsbF	Ser F12 – Arg F45	ACE,[b] NONE [c]	HEM F101	–
PsbI	Met I1 - Asp I36	NONE, [e] CT3 [d]	–	–
PsbJ	Gly J5 – Leu J40	ACE,[b] NONE [c]	MG J101	–
PsbX	Thr X2 – Arg X39	NTER, [f] CT3 [d]	–	–

[a] Based on CHARMM.[3,4] [b] Pseudo N-terminus. [c] Real C-terminus. [d] Pseudo C-terminus. [e] Real N-terminus, formylated. [f] Real N-terminus.

We note that RC preparations are expected to contain the peptides PsbA, PsbD, PsbE, PsbF, and PsbI.[5-8] The presently used full model contains PsbX as well in order to test a possible influence on the site energy of $Chlz_{D2}$ as compared to the influence of the symmetry-related PsbI on $Chlz_{D1}$. The inclusion of PsbJ and PsbY (the latter not present in 3WU2) is for later applications of the model concerning the redox properties of cytochrome b_{559}.[9] Of the water molecules present in the crystal structures, only six in the vicinity of Chl_{D1}/Chl_{D2} were explicitly modeled. These are the water molecules forming the axial ligands to Chl_{D1}/Chl_{D2} as well as the two water molecules being in hydrogen bonding contact with the axial ligands (see Figure 2 of the main

text). In addition, two water molecules were considered that form hydrogen bonds to the 13^1-keto groups of Chl_{D1}/Chl_{D2} and the histidine side chains being the axial ligands to P_{D1}/P_{D2}. All these water molecules were included because of their vicinity to Chls and because they are expected to have a relatively fixed orientation due to their involvement in hydrogen bonding networks, so that an explicit modeling in the framework of the Poisson-Boltzmann approach is appropriate. This was done only for 3WU2, because the corresponding water molecules in 4PJ0 were not completely assigned, which is a consequence of the lower resolution of the latter crystal structure.

Table S2: Structural elements contained in the full RC model based on PDB 4PJ0 (*T. elongatus*).

Peptide	Modeled amino acids	Patches [a]	Cofactors	Explicit water molecules
PsbA	Asn A12 – Ala A344	ACE,[b] NONE [c]	OEX A601, FE A602, LMG A603, CL A604, A605, CLA A 606 – A608, BCR A609, PL9 610, SQD A611, LMG A612, LHG A613, A614, SO4 A615, BCT A616, DGD C516 – C518, H102	–
PsbD	Gly D13 – Leu D352	ACE,[b] NONE [c]	PHO D401, D402, CLA D403 – D405, BCR D406, PL9 D407, LHG D408, LMG D409	–
PsbE	Ala E2 – Leu E83	NTER, [d] CT3 [e]	LHG E101, HEM E102, LHG L102	–
PsbF	Tyr F13 – Arg F45	ACE,[b] NONE [c]	SQD F101	–
PsbI	Met I1 - Lys I33	NONE, [f] CT3 [d]	–	–
PsbJ	Arg J7 – Leu J40	ACE,[b] NONE [c]	–	–
PsbY	Asp R2 – Leu R35	NONE, [f] CT3 [d]	–	–
PsbX	Thr X2 – Glu X38	NTER, [f] CT3 [d]	–	–

[a] Based on CHARMM.[3,4] [b] Pseudo N-terminus. [c] Real C-terminus. [d] Real N-terminus. [e] Pseudo C-terminus. [f] Real N-terminus, formylated.

In the Poisson-Boltzmann approach, protein and cofactors are modeled as a set of atomic partial charges (APCs) embedded in a dielectric medium. For heavy atoms, the positions of APCs are inferred from crystal structure coordinates. The positions of hydrogen atoms are determined by modeling with CHARMM.[3,4] APCs for protein parts, β-carotene, and the heme group are taken from the CHARMM force field,[10] while those for the ground and first excited states of Chl *a* and Pheo *a* are determined based on quantum chemical computations of the pigments *in vacuo* as

detailed below (S2). For the initial CHARMM computations serving to add hydrogen atoms, we use the ground state APCs from Ishikita and Knapp for Chl *a*[11] and Pheo *a*.[12] APCs for other cofactors are likewise taken from the work of Ishikita et al., in particular, for neutral and reduced plastoquinone as well as bicarbonate[12] and for lipids.[11,13] APCs for the sulfate ion in 4PJ0 were taken from Cannon et al.[14] Preliminary APCs assigned to the WOC (OEX) are +3.5 for Mn, –2.0 for O, and +2.0 for Ca. These APCs were varied in order to test a possible effect of net charge changes in the region of the WOC on site energies, but are not meant to represent any realistic charge distribution within the WOC.

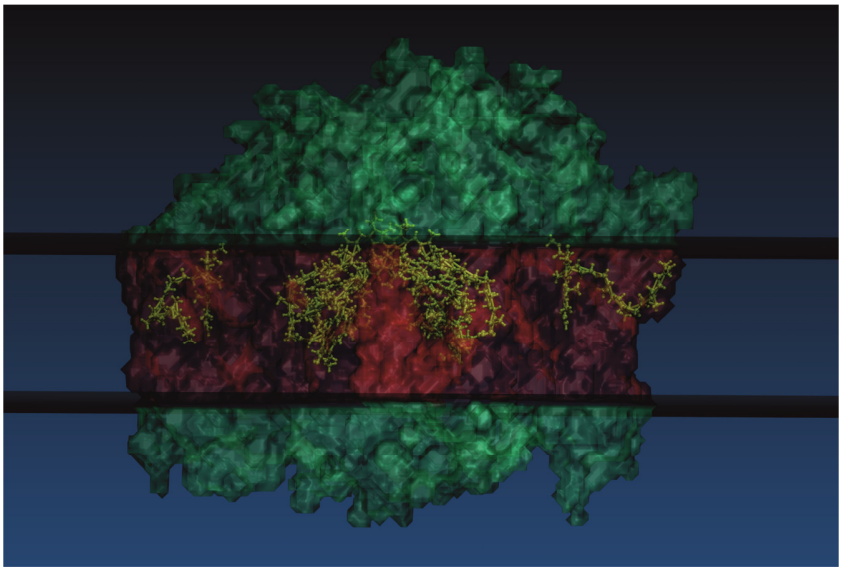

Figure S1: Arrangement of chlorin pigments in the RC of PSII relative to the boundary surfaces between regions of space, to which different dielectric constants are assigned in the electrostatic model. These constants are $\varepsilon_p = 4.0$ and $\tilde{\varepsilon}_p = 1.5$ for protonation states and site energy shifts, respectively, in the protein interior, $\varepsilon_{mem} = 2.0$ in the membrane slab, and $\varepsilon_{solv} = 80$ in the surrounding solvent. Figure made with VMD.[15]

The dielectric medium is divided into four regions as illustrated in Figure S1: a volume occupied by the PPC atoms thus harboring all APCs, two regions occupied by solvent, and a region representing the interior of the thylakoid membrane (also used as approximation for the interior of a detergent belt). To these regions, static dielectric constants ε_p, ε_{solv}, and ε_{mem}, respectively, are assigned, so that the dielectric function $\varepsilon(\mathbf{r})$ is piecewise constant. The choice of particular values for these dielectric constants is discussed below (S3).

Poisson-Boltzmann calculations are carried out by using the TAPBS front-end[16] connected to the Adaptive Poisson-Boltzmann Solver APBS.[17] In TAPBS, a membrane slab is defined by two points in space represented by two vectors. One vector points from the origin of the coordinate system to a point in one of the two plains dividing the membrane interior from the solvent region (cf. Figure S1). The second vector points from the latter position to a point in the second plain, is normal to the plains, and its length defines the thickness of the slab. For the RC of PSII, the first point was chosen as the position of the nonheme iron and the second point as the average of the positions of the Mg ions of P_{D1} and P_{D2}, resulting in a membrane slab having a thickness of 27 Å. This slab was then shifted by 2 Å towards the lumenal side to achieve a better match of the

membrane interior with the positions of the hydrophobic tails of structural lipids. The resulting membrane slab is shown in Figure S1. In the case of 4PJ0, the original membrane slab was used, but shifting the membrane slab has a marginal effect on site energies as shown below (S8).

S2: Quantum chemistry and computation of atomic partial charges for Chl *a* and Pheo *a*

The PBQC method requires APCs representing the electronic ground and first excited states of the pigments whose site energy shifts are to be computed.[18,19] To obtain these APCs, quantum chemical computations of Chl *a* and Pheo *a in vacuo* were carried out by using Q-CHEM 4.0.1.[20] Geometry optimization was performed with DFT using the B3LYP exchange correlation (XC) functional and the 6-31g(d,p) basis set. In the optimized structures, the 3-vinyl group points towards the C2 ring atom corresponding to a C2-C3-$C3^1$-$C3^2$ torsional angle of – 30.3° for Chl *a* and 31.2° for Pheo *a*. The optimized coordinates are used to create a 3D grid around the molecule by CHELP-BOW.[21] This grid consists of 2500 points per atom sampled randomly from 0 to a maximum of 8 Å from any atom. Ground and excited state wavefunctions were computed by using the Hartree-Fock configuration interaction singles (HF-CIS) method and the 6-31g* basis set, providing the electrostatic potential (ESP) for each point on the 3D grid. Finally, CHELP-BOW[21] is used to calculate APCs for each atom by a weighted least-squares fit to the ESP. The resulting APCs are compiled in Table S3. This charge fitting procedure results in suitable APCs for a highly accurate computation of intermolecular couplings as shown earlier by a comparison with a direct numerical evaluation of the Coulomb integrals.[22] We note that transition energies from quantum chemistry are not used in the PBQC method. The difference dipole $\Delta\boldsymbol{\mu}$, i.e., the difference in first moment of the APCs between S_1 and S_0 state is 1.10 D for Chl *a* and 1.59 D for Pheo *a*. These values are in reasonable agreement with experimental data based on Stark effect measurements, yielding $\Delta\boldsymbol{\mu}$ = 0.9 – 1.0 D f^{-1} for Chl *a*[23] and 1.5 D f^{-1} for Pheo *a*.[24] Here, f^{-1} is a local field correction factor.

Besides HF-CIS, we tested alternative electronic structure methods to produce APCs based on time-dependent- (TD) DFT[25] with various XC-functionals such as the formerly used BHHLYP and B65LYP[26] employing the Tamm-Dancoff approximation (TDA)[27] as well as CAM-B3LYP[28] with TDA or random phase approximation (RPA).[25] Based on a comparison of simulated and experimental optical spectra, we found the results obtained with the TD-DFT methods less satisfactory. Therefore, we focus in the present work on data obtained with the HF-CIS method.

S3: Protonation states and site energies

In the present work, a refined version of the PBQC method is introduced, in which protonation states of titratable groups in the protein matrix and the site energies of protein-bound pigments are evaluated simultaneously using different protein dielectric constants for the protonation states and site energies. This refinement is explained in the following.

Since each titratable site μ has (at least) two possible protonation states, a PPC with N such sites has (at least) 2^N possible protonation patterns.[19,29] Each pattern can be characterized by a vector

$$\mathbf{x}_\sigma = \left(x_1^{(\sigma)}, x_2^{(\sigma)}, ..., x_N^{(\sigma)}\right) \quad (1)$$

where $x_\mu^{(\sigma)} = 1$, if site μ is protonated, $x_\mu^{(\sigma)} = 0$, if site μ is deprotonated, and σ = 1, …, 2^N counts the protonation patterns.

Table S3: Atomic partial charges of the electronic ground (S_0) and first excited (S_1, Q_Y) states of Chl *a* and Pheo *a* determined by using the HF-CIS method.

Atom	Chl *a* S_0	Chl *a* S_1	Pheo *a* S_0	Pheo *a* S_1
MG	1.100	1.105	–	–
HNB	–	–	0.364	0.378
HND	–	–	–0.082	–0.094
CHA	0.282	0.321	0.280	0.290
CHB	–0.672	–0.617	–0.661	–0.612
HHB	0.190	0.182	0.204	0.195
CHC	–0.090	–0.145	–0.124	–0.172
HHC	0.116	0.120	0.131	0.133
CHD	–0.050	–0.272	0.097	–0.082
HHD	0.141	0.159	0.125	0.139
NA	–0.612	–0.614	–0.354	–0.356
C1A	–0.033	–0.038	–0.165	–0.153
C2A	0.198	0.201	0.038	0.025
H2A	–0.003	–0.003	0.065	0.068
C3A	0.017	0.015	0.277	0.281
H3A	0.040	0.039	–0.028	–0.030
C4A	0.583	0.569	0.417	0.397
CMA	–0.414	–0.407	–0.458	–0.455
HMA1,2,3	0.115	0.114	0.112	0.111
CAA	0.116	0.116	0.237	0.248
HAA1,2	–0.027	–0.027	–0.026	–0.028
CBA	–0.253	–0.251	–0.550	–0.552
HBA1,2	0.030	0.029	0.120	0.121
CGA	0.912	0.913	0.965	0.965
O1A	–0.622	–0.622	–0.624	–0.624
O2A	–0.412	–0.412	–0.413	–0.414
NB	–0.525	–0.506	–0.398	–0.393
C1B	0.303	0.231	0.311	0.250
C2B	0.186	0.175	0.170	0.163
C3B	0.023	–0.023	–0.028	–0.079
C4B	0.045	0.104	0.077	0.129
CMB	–0.522	–0.520	–0.510	–0.509
HMB1,2,3	0.151	0.150	0.151	0.151
CAB	–0.185	–0.177	–0.109	–0.100
HAB	0.159	0.157	0.133	0.132
CBB	–0.355	–0.368	–0.379	–0.393
HBB1,2	0.175	0.177	0.182	0.183
NC	–0.337	–0.426	–0.124	–0.193
C1C	–0.076	–0.030	–0.089	–0.055
C2C	0.285	0.304	0.307	0.310
C3C	–0.194	–0.215	–0.231	–0.243
C4C	–0.008	0.201	–0.097	0.077
CMC	–0.595	–0.594	–0.640	–0.636
HMC1,2,3	0.164	0.164	0.175	0.175
CAC	0.149	0.149	0.220	0.220

Table S3 (continued)

Atom	Chl *a* S_0	Chl *a* S_1	Pheo *a* S_0	Pheo *a* S_1
HAC1,2	0.000	–0.001	–0.024	–0.024
CBC	–0.180	–0.179	–0.152	–0.150
HBC1,2,3	0.047	0.047	0.036	0.036
ND	–0.487	–0.538	0.295	0.268
C1D	–0.006	0.180	–0.329	–0.176
C2D	0.233	0.168	0.328	0.276
C3D	–0.288	–0.289	–0.311	–0.300
C4D	0.089	0.115	–0.170	–0.144
CMD	–0.464	–0.455	–0.465	–0.458
HMD1,2,3	0.143	0.141	0.143	0.141
CAD	0.783	0.791	0.753	0.749
OBD	–0.552	–0.554	–0.553	–0.552
CBD	–0.858	–0.914	–0.687	–0.702
HBD1	0.240	0.253	0.245	0.248
CGD	0.954	0.962	0.831	0.836
O1D	–0.606	–0.606	–0.566	–0.567
O2D	–0.362	–0.358	–0.331	–0.331
CED	–0.176	–0.178	–0.158	–0.159
HED1,2,3	0.124	0.124	0.119	0.119
C1	–0.146	–0.146	–0.132	–0.132
H1,2	0.1755	0.1755	0.168	0.168

In thermal equilibrium, the protonation probability of group μ is $\langle x_\mu \rangle_\sigma$, where

$$\langle A(\sigma) \rangle_\sigma = \frac{\sum_{\sigma=1}^{2^N} A(\sigma) \exp\left[-\frac{G_\sigma}{k_B T}\right]}{\sum_{\sigma=1}^{2^N} \exp\left[-\frac{G_\sigma}{k_B T}\right]} \tag{2}$$

is the Boltzmann average of a protonation pattern dependent quantity $A(\sigma)$ over all protonation patterns. Here, G_σ is the Gibbs free energy of pattern σ, k_B is Boltzmann´s constant, and T is the absolute temperature.

In the framework of the PBQC method as implemented in the present work, the site energy of pigment m in the PPC, E_m, is given as

$$E_m = \langle E'_m(\sigma) \rangle_\sigma + E_\lambda \tag{3}$$

where $E'_m(\sigma)$ is the (protonation pattern dependent) energy difference between excited and ground state of pigment m, when both are fully equilibrated, and E_λ is the reorganization energy of the optical transition assumed to be m-independent. Because of electrostatic pigment-protein interactions, the energy difference between excited and ground state depends on the charge states of the titratable sites, which can be expressed as[19]

$$E'_m(\sigma) = E'_m(0) + \sum_{\mu=1}^{N} W_{m\mu} \left(x_\mu^{(\sigma)} + z_\mu \right) \tag{4}$$

Here, $E'_m(0)$ is the site energy obtained for a reference protonation pattern, in which all titratable sites are in their charge neutral state, $W_{m\mu}$ is the electrostatic interaction energy between pigment m and titratable site μ, and z_μ is a formal charge number that ensures that the term $W_{m\mu}(x_\mu^{(\sigma)} + z_\mu)$ is non-zero only, when group μ is charged. The electrostatic correction for non-reference protonation patterns reads explicitly

$$W_{m\mu} = \sum_{\beta \in \Phi} \left(Q_{\beta,\mu}^{(\mathrm{h})} - Q_{\beta,\mu}^{(\mathrm{d})}\right)\left(\phi_{\mathrm{p},m}^{(1)}(\mathbf{R}_\beta) - \phi_{\mathrm{p},m}^{(0)}(\mathbf{R}_\beta)\right) \tag{5}$$

In this equation, $Q_{\beta,\mu}^{(\mathrm{h})}$ and $Q_{\beta,\mu}^{(\mathrm{d})}$ are the APCs assigned to atom β of titratable group μ in its protonated (h) and deprotonated (d) state, respectively. The set Φ contains all atoms of group μ, for which $Q_{\beta,\mu}^{(\mathrm{h})} \neq Q_{\beta,\mu}^{(\mathrm{d})}$. The electrostatic potentials $\phi_{\mathrm{p},m}^{(1)}(\mathbf{R}_\beta)$ and $\phi_{\mathrm{p},m}^{(0)}(\mathbf{R}_\beta)$ are those produced by the APCs of the first excited and ground state, respectively, of the pigment m in the dielectric environment of the PPC (index p) represented by the three dielectric constants $\tilde{\varepsilon}_\mathrm{p}$, ε_mem, and $\varepsilon_\mathrm{solv}$ defining $\varepsilon(\mathbf{r})$ as described above (cf. Figure S1). These potentials are obtained as solutions to the linearized Poisson-Boltzmann equation (LPBE)

$$\nabla\left(\varepsilon(\mathbf{r})\nabla\phi(\mathbf{r})\right) = -\frac{1}{\varepsilon_0}\sum_{\alpha \in \Omega} q_\alpha^{(m)}(a,a)\,\delta(\mathbf{r} - \mathbf{R}_\alpha) + \kappa^2(\mathbf{r})\,\phi(\mathbf{r}) \qquad (a = 0, 1) \tag{6}$$

which is solved numerically using finite difference techniques[30] employing TAPBS.[16] Here, $q_\alpha^{(m)}(a,a)$ is the APC assigned to atom α of pigment m at position $\mathbf{R}_\alpha$ in the electronic state a of the pigment (see Table S3). The set Ω contains all atoms of pigment m, for which $q_\alpha^{(m)}(0,0) \neq q_\alpha^{(m)}(1,1)$. κ is the inverse Debye length, which is related to the ionic strength $I(\mathbf{r})$ of the solution by $\kappa^2(\mathbf{r}) = e^2 N_\mathrm{A} 2I(\mathbf{r})/(\varepsilon(\mathbf{r})\varepsilon_0 k_\mathrm{B} T)$. The ionic strength is position-dependent, because the ions are assumed to neither penetrate the protein volume nor the membrane interior. The solutions of the LPBE in eq. (6) also enter the two contributions $\Delta\Delta G_\mathrm{back}^{(m)}$ and $\Delta\Delta G_\mathrm{pol}^{(m)}$ to $E'_m(0)$,[19] i.e.

$$E'_m(0) = E'_0 + \Delta\Delta G_\mathrm{back}^{(m)} + \Delta\Delta G_\mathrm{pol}^{(m)} \tag{7}$$

Here, the "background term" $\Delta\Delta G_\mathrm{back}^{(m)}$ represents interactions of the pigment´s APCs with background charges (i.e., ground state APCs of the environment), while the "polarization term" $\Delta\Delta G_\mathrm{pol}^{(m)}$ (also referred to as "Born term") represents interactions of the pigment´s APCs with the reaction field they induce in the dielectric environment. E'_0 in eq. (7) is the transition energy of the pigment in an aqueous solvent.

In these calculations, we use routinely $\varepsilon_\mathrm{mem} = 2.0$ and $\varepsilon_\mathrm{solv} = 80$. $\tilde{\varepsilon}_\mathrm{p}$ is an empirical constant that is not simply the effective dielectric constant of the protein interior but also serves to tune the Coulomb interaction between pigment and protein such as to match the different sets of APCs employed for the two parts. In this way, possible errors due to shortcomings of quantum chemically computed charge distributions can be counterpoised. We found that when using pigment APCs derived from HF-CIS (Table S3) together with protein APCs from the CHARMM force field, a value of $\tilde{\varepsilon}_\mathrm{p} = 1.5$ gives good results.

In order to compute the average $\langle E'_m(\sigma)\rangle_\sigma$, the Gibbs free energy G_σ is required:[19,29]

$$G_\sigma = \sum_{\mu=1}^{N}\left(x_\mu^{(0)} - x_\mu^{(\sigma)}\right)\Delta G_\mathrm{p}(\mathrm{A}_\mu\mathrm{H}, \mathrm{A}_\mu) + \frac{1}{2}\sum_{\mu,\nu=1}^{N} W_{\mu\nu}\left(x_\mu^{(\sigma)} + z_\mu\right)\left(x_\nu^{(\sigma)} + z_\nu\right) \tag{8}$$

Here

$$\Delta G_{\mathrm{p}}(\mathrm{A}_{\mu}\mathrm{H},\mathrm{A}_{\mu}) = k_{\mathrm{B}}T\,\ln 10\,(\mathrm{p}K_{\mathrm{a}} - \mathrm{pH}) + \Delta\Delta G_{\mathrm{back}}^{(\mu)} + \Delta\Delta G_{\mathrm{pol}}^{(\mu)} \tag{9}$$

is the Gibbs free energy difference between the protonated ($\mathrm{A}_{\mu}\mathrm{H}$) and the deprotonated ($\mathrm{A}_{\mu}$) state of the protein-bound group μ at a given pH of the surrounding solution (defined as the reaction free energy for the deprotonation reaction) and with all the remaining titratable sites in their charge neutral states. In eq. (9), pK_{a} is the reference pK_{a}-value of the titratable group in an aqueous solution determined experimentally.[29] The intrinsic pK_{a}-value of a titratable group in the protein is defined by[29]

$$\mathrm{p}K_{\mathrm{int}}^{(\mu)} = \mathrm{p}K_{\mathrm{a}} - \frac{1}{k_{\mathrm{B}}T\ln 10}\left(\Delta\Delta G_{\mathrm{back}}^{(\mu)} + \Delta\Delta G_{\mathrm{pol}}^{(\mu)}\right) \tag{9}$$

and also refers to the hypothetical situation that all other titratable groups are in their uncharged state. The second term in eq. (8) is a correction for the interaction between charged groups μ and ν. This interaction is given by

$$W_{m\mu} = \sum_{\beta\in\Phi}\left(Q_{\beta,\mu}^{(\mathrm{h})} - Q_{\beta,\mu}^{(\mathrm{d})}\right)\left(\phi_{\mathrm{p},\mu}^{(\mathrm{d})}(\mathbf{R}_{\beta}) - \phi_{\mathrm{p},\mu}^{(\mathrm{h})}(\mathbf{R}_{\beta})\right) \tag{10}$$

with the potentials originating from the LPBE

$$\nabla\left(\varepsilon(\mathbf{r})\nabla\phi(\mathbf{r})\right) = -\frac{1}{\varepsilon_0}\sum_{\beta\in\Phi} Q_{\beta,\mu}^{(\mathrm{i})}\,\delta(\mathbf{r}-\mathbf{R}_{\beta}) + \kappa^2(\mathbf{r})\,\phi(\mathbf{r}) \qquad (\mathrm{i} = \mathrm{h},\mathrm{d}) \tag{11}$$

These potentials also enter the two contributions $\Delta\Delta G_{\mathrm{back}}^{(\mu)}$ and $\Delta\Delta G_{\mathrm{pol}}^{(\mu)}$ to $\Delta G_{\mathrm{p}}(\mathrm{A}_{\mu}\mathrm{H},\mathrm{A}_{\mu})$ in eq. (9).[29] In these calculations, values of $\varepsilon_{\mathrm{mem}} = 2.0$, $\varepsilon_{\mathrm{solv}} = 80$, and $\varepsilon_{\mathrm{p}} = 4.0$ are routinely applied. The latter value was found to be a reasonable approximation in conjunction with the CHARMM force field.[31,32] Note that $\varepsilon_{\mathrm{p}} \neq \tilde{\varepsilon}_{\mathrm{p}}$.

The average $\langle E_m'(\sigma)\rangle_{\sigma}$ is computed by Monte Carlo (MC) importance sampling based on the Metropolis criterion[33] as implemented in the software Karlsberg2.[34] The crucial point in the refined PBQC method used here is that the average $\langle E_m'(\sigma)\rangle_{\sigma}$ is evaluated by computing G_{σ} with $\varepsilon_{\mathrm{p}} = 4.0$ and at the same time $E_m'(\sigma)$ with $\tilde{\varepsilon}_{\mathrm{p}} = 1.5$. This is achieved by combining the output of two different Poisson-Boltzmann calculations using TAPBS into one input to the MC simulation using Karlsberg2 as illustrated in Figure S2. In this way, the importance sampling of protonation patterns can be performed with the optimal value of ε_{p} for the computation of G_{σ} and for each protonation pattern, $E_m'(\sigma)$ can be computed with an independent optimal value for $\tilde{\varepsilon}_{\mathrm{p}}$.

Because of the use of finite difference techniques,[30] the PBQC method only produces shifts of site energies with respect to E_0' in eq. (7).[19] This latter transition energy is arbitrarily set to zero, and the actual site energy is computed as

$$E_m = \langle E_m'(\sigma)\rangle_{\sigma} + E_0 \tag{12}$$

where the offset E_0 ($\neq E_0'$) is determined from a comparison of simulated and measured spectra. Note that this offset also accounts for the site-independent reorganization energy E_{λ} in eq. (3), so that E_m can be interpreted as vertical transition energy. If there are two chemically different types of pigments in the PPC such as Chl *a* and Pheo *a* in the RC of PSII, two independent values of E_0 have to be specified, one for each pigment type.

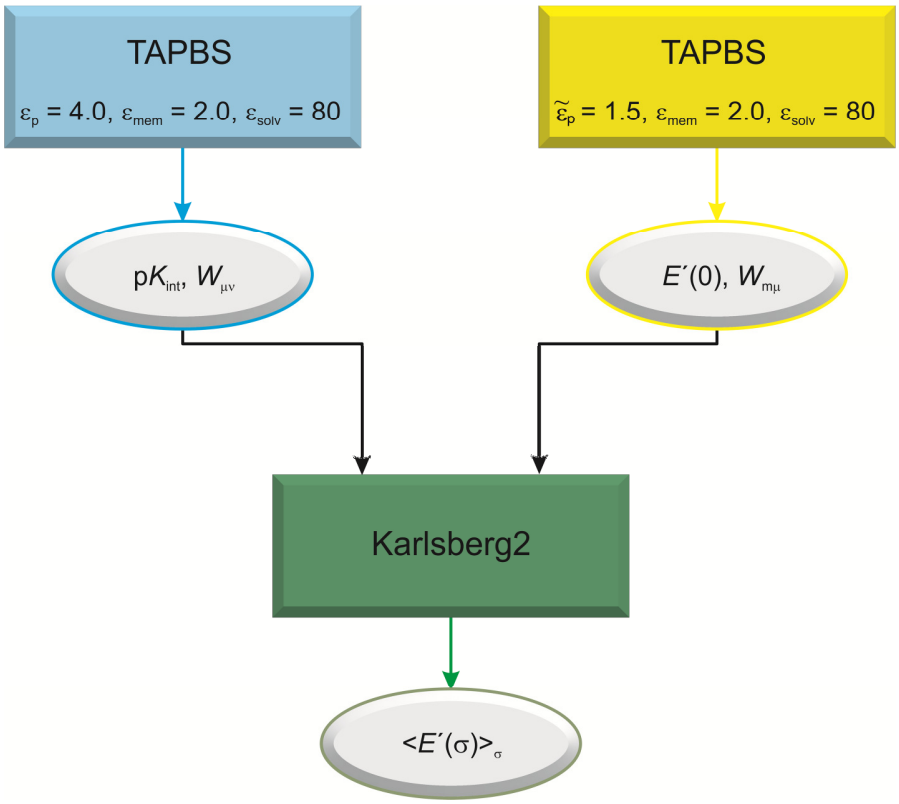

Figure S2: Flowchart illustrating the combination of two different TAPBS computations to produce the input for the MC sampling in Karlsberg2 using simultaneously different values for the effective dielectric constant of the protein, i.e., $\varepsilon_p = 4.0$ for the intrinsic pK_a values pK_{int} of titratable groups and electrostatic interactions $W_{\mu\nu}$ between charged titratable groups as well as $\tilde{\varepsilon}_p = 1.5$ for the site energy shifts $E'(0)$ of pigments and electrostatic interactions $W_{m\mu}$ between pigments and charged titratable groups.

S4: Simulation of linear optical spectra

The simulation of linear optical spectra, i.e., absorption (OD, optical density), linear dichroism (LD), circular dichroism (CD), and fluorescence, is based on the dynamical theory of optical spectra delineated in detail elsewhere[35] and is performed as described by Raszewski et al.[36,37] Starting point of the spectral simulation is the exciton Hamiltonian in eq. (1) of the main text with the site energies E_m as diagonal elements and the excitonic couplings V_{mn} as off-diagonal elements. The latter couplings are taken from Shibata et al.[38] and were computed by using the Poisson-TrEsp method[39-41] with the exception of the coupling between P_{D1} and P_{D2}, which was set to 158 cm^{-1} to account for the consequences of some electron exchange between these two pigments.[41] For convenience, these excitonic couplings are reproduced in Table S4.

The site energy values E_m from eq. (12) are used as diagonal elements in the exciton matrix. This procedure is a reasonable approximation, if the distribution of site energies over protonation patterns in narrow.[19] Below, it is demonstrated that this is the case for the RC of PSII (S9).

Table S4: Excitonic couplings V_{mn} between pigments in the RC of PSII from Shibata et al.[38] used in the present work.

Pigment m	Pigment n	V_{mn} in cm^{-1}	Pigment m	Pigment n	V_{mn} in cm^{-1}
1 P_{D1}	2 P_{D2}	158.00	3 Chl_{D1}	5 $Pheo_{D1}$	43.51
1 P_{D1}	3 Chl_{D1}	–27.32	3 Chl_{D1}	6 $Pheo_{D2}$	–2.18
1 P_{D1}	4 Chl_{D2}	–41.83	3 Chl_{D1}	7 $Chlz_{D1}$	1.67
1 P_{D1}	5 $Pheo_{D1}$	–3.96	3 Chl_{D1}	8 $Chlz_{D2}$	–0.09
1 P_{D1}	6 $Pheo_{D2}$	12.61	4 Chl_{D2}	5 $Pheo_{D1}$	–2.37
1 P_{D1}	7 $Chlz_{D1}$	0.45	4 Chl_{D2}	6 $Pheo_{D2}$	41.65
1 P_{D1}	8 $Chlz_{D2}$	0.58	4 Chl_{D2}	7 $Chlz_{D1}$	–0.05
2 P_{D2}	3 Chl_{D1}	–46.77	4 Chl_{D2}	8 $Chlz_{D2}$	1.80
2 P_{D2}	4 Chl_{D2}	–22.04	5 $Pheo_{D1}$	6 $Pheo_{D2}$	1.55
2 P_{D2}	5 $Pheo_{D1}$	15.06	5 $Pheo_{D1}$	7 $Chlz_{D1}$	–2.52
2 P_{D2}	6 $Pheo_{D2}$	–2.99	5 $Pheo_{D1}$	8 $Chlz_{D2}$	–0.18
2 P_{D2}	7 $Chlz_{D1}$	0.60	6 $Pheo_{D2}$	7 $Chlz_{D1}$	–0.19
2 P_{D2}	8 $Chlz_{D2}$	0.61	6 $Pheo_{D2}$	8 $Chlz_{D2}$	–2.57
3 Chl_{D1}	4 Chl_{D2}	3.54	7 $Chlz_{D1}$	8 $Chlz_{D2}$	0.15

To avoid spurious excitonic coherences between weakly coupled pigments, exciton domains are introduced as described earlier[38,42] by using a threshold value of V_c = 30 cm^{-1}. A glance at Table S4 shows that with this threshold value, the six RC pigments P_{D1}, P_{D2}, Chl_{D1}, Chl_{D2}, $Pheo_{D1}$, and $Pheo_{D2}$ form one exciton domain, while $Chlz_{D1}$ and $Chlz_{D2}$ form two single-pigment domains. The exciton coefficients are obtained from a diagonalization of the 6 × 6 submatrix of the inner RC pigments.

The spectral line shape depends on the coupling of Q_Y transitions to protein vibrational modes, which is characterized by the spectral density[35,36]

$$J(\omega) = \sum_{i=1}^{2} \frac{s_i}{7!\,2\omega_i^4}\,\omega^3 \exp\left[-\left(\frac{\omega}{\omega_i}\right)^{1/2}\right] \tag{13}$$

with s_1 = 0.4, s_2 = 0.25, ω_1 = 20 cm^{-1} , and ω_2 = 70 cm^{-1}, resulting in an overall Huang-Rhys factor of 0.65. Inhomogeneous broadening is accounted for by a MC method, in which site energies are drawn from a Gaussian distribution with center E_m and FWHM Δ_{inh} = 180 cm^{-1}. In some cases, smaller values of Δ_{inh} are used for specific pigments. We note that the MC method to simulate inhomogeneous broadening is independent of the MC method to sample protonation patterns and accounts for site energy distributions due to slow conformational variations of the protein matrix.

The transition dipoles used in the simulations of spectral intensities are 5.47 D for Chl *a* and 4.25 D for Pheo *a*. These values originate from an analysis of the Chl *a* dipole strengths in various solvents,[43] assuming that the protein matrix has an optical dielectric constant of $\varepsilon_{opt} = 2.0$,[44] and taking into account the different dipole strengths for Chl *a* and Pheo *a* as measured in ether solvent.[45] To simulate spectra of mutant RCs, in which $Pheo_{D1}$ is replaced with Chl, a correspondingly increased transition dipole is assigned to the $Pheo_{D1}$ site and all excitonic couplings involving this site are scaled by the factor 5.47/4.25. Spectra of RCs with a triplet state localized on a particular pigment are simulated by setting the dipole strength of this pigment as well as all excitonic couplings involving this pigment to zero.

In Figure 5 of the main text, we use the exciton state pigment distribution function d_m and the density of exciton states D_M to illustrate the consequences of exciton delocalization between the six inner pigments of the RC. These functions are given by

$$d_m(\omega) = \left\langle \sum_M \left| c_m^{(M)} \right|^2 \delta(\omega - \omega_M) \right\rangle_{\text{dis}} \tag{14}$$

where $\hbar\omega_M$ is the vertical transition energy of exciton state M and $\langle ... \rangle_{\text{dis}}$ indicates an average over static site energy disorder, and

$$D_M(\omega) = \left\langle \delta(\omega - \omega_M) \right\rangle_{\text{dis}} \tag{15}$$

These functions are shown in the left part of Figure 5 converted to the wavelength scale.

S5: Compilation of computed site energy shifts

Table S5: Site energy shifts $\langle E'_m(\sigma) \rangle_\sigma = E_m - E_0$ in cm^{-1} calculated based on different structural models.

Pigment *m*	4PJ0	3WU2						
	full [a]	full [b] conf. I [c]	full [b] conf. II [d]	del. PsbI [d,e]	del. PsbJ [d,f]	del. PsbX [d,g]	del. H_2O [h]	del. WOC [d,i]
1 P_{D1}	−118	−107	−106	−107	−106	−107	−106	−105
2 P_{D2}	−106	−112	−120	−120	−120	−121	−92	−119
3 Chl_{D1}	−299	−329	−300	−297	−300	−300	−272	−320
4 Chl_{D2}	−172	−188	−187	−188	−187	−189	−84	−189
5 $Pheo_{D1}$	25	85	60	63	61	62	48	76
6 $Pheo_{D2}$	−63	−28	−28	−27	−26	−27	−62	−25
7 $Chlz_{D1}$	−196	−246	−246	−264	−246	−246	−246	−246
8 $Chlz_{D2}$	−80	−150	−150	−150	−151	−143	−151	−150

[a] Full model containing all structural elements listed in Table S2 (no explicit water). [b] Full model containing all structural elements listed in Table S1. [c] Arrangement of water molecules near Chl_{D1} as shown in Figure S3A. [d] Arrangement of water molecules near Chl_{D1} as shown in Figure S3B. [e] Without PsbI. [f] Without PsbJ. [g] Without PsbX. [h] Without explicit water. Arrangement of the hydroxyl group of Thr A179 as shown in Figure S3A. [i] Without WOC (i.e., without the atoms assigned to OEX).

S6: Contributions to site energy shifts of Chl_{D1}/Chl_{D2}

Table S6: Contribution of selected protein parts and explicit water molecules to the site energy shifts of Chl_{D1}/Chl_{D2} (in cm^{-1}).

Group	Chl_{D1}	Chl_{D2}	Group	Chl_{D1}	Chl_{D2}	Group	Chl_{D1}	Chl_{D2}
Loop [a] BB [b]	0	–15	Asn A181	0	0	H_2O 930 [e]	–3	–3
SC [c]	–1	–12	Arg D180	3	39	H_2O 931 [f]	0	–71
Helix [d] BB [b]	18	26	Met A183	19	0	H_2O 932 [g], conf. I	12	0
SC [c]	58	36	Leu D182	0	–3	H_2O 932 [g], conf. II	–41	0
Met A172	–53	0	Gln A199	1	–1	H_2O 933 [h], conf. I	–64	1
Pro D171	0	7	Met D198	1	0	H_2O 933 [h] conf. II	–71	0
Pro A173	–1	0	Leu A200	0	–1	H_2O 934 [i]	0	–27
Ser D172	0	4	Met D199	0	0	H_2O 935 [j]	–1	–2
Ser A177	1	0	Thr A179, conf. I	–25	0	Ile D178	0	14
Ala D176	0	–2	Thr A179, conf. II	62	0			

[a] Met A172 – Ile A176 for Chl_{D1}; Pro D171 – Val D175 for Chl_{D2}. [b] Backbone. [c] Side chains. [d] Ser A177 – His A190 for Chl_{D1}; Ala D176 – His D189 for Chl_{D2}. [e] Hydrogen bond to 13^1-keto group of Chl_{D2}. [f] Hydrogen bond to 13^3-methyl ester of Chl_{D2}. [g] Axial ligand to Chl_{D1}. [h] Hydrogen bond to 13^3-methyl ester of Chl_{D1}. [i] Axial ligand to Chl_{D2}. [j] Hydrogen bond to 13^1-keto group of Chl_{D1}.

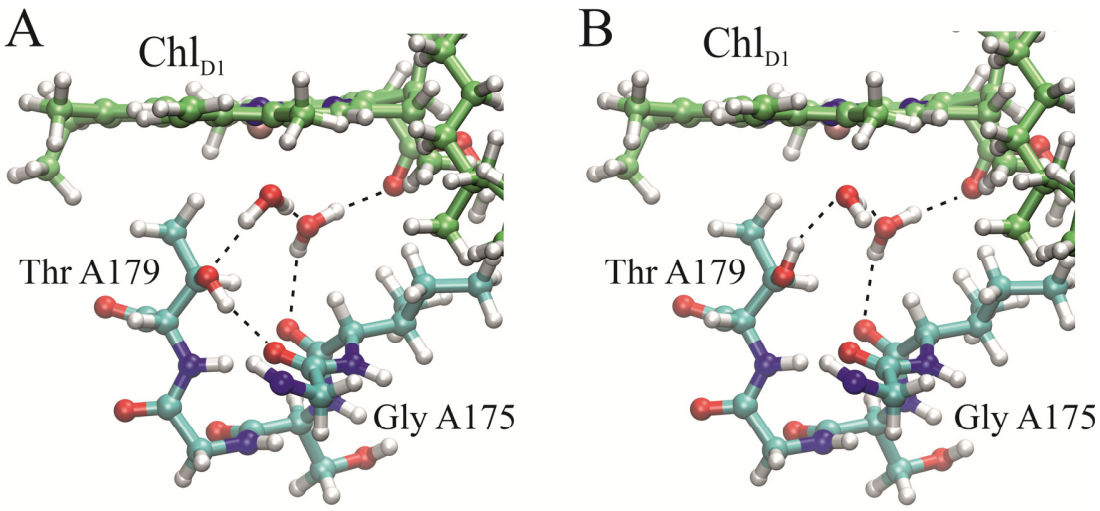

Figure S3: Arrangement of water molecules near Chl_{D1} in conformation I (A; same as in Figure 2A of the main text) compared to conformation II (B). The protein segment shown is Gly A175 to Thr A179. Color code: carbon, green (Chl) and cyan (protein); oxygen, red; nitrogen, blue; hydrogen, white. The black dashed lines indicate hydrogen bonds. Figure made with VMD[15] based on PDB 3WU2[1] with hydrogen atoms modeled by using CHARMM.[3,4,10]

S7: Comparison of various simulated spectra with experiment

Table S7: Site energies E_m in nm (values in parentheses in cm^{-1}) used in various spectral simulations in the present work.

Pigment *m*	I RC	II RC presumably containing Q_A	III RC mutant LH(D209)	IV PSIIcc with neutral Q_A	V PSIIcc with Q_A reduced	VI Shift due to reduction of Q_A [d]
1 P_{D1}	668 (14970)	668 (14970)	668 (14970)	668 (14970)	668 (14970)	(4)
2 P_{D2}	668 (14970)	668 (14970)	668 (14970)	668 (14970)	667.4 (14984)	(14)
3 Chl_{D1}	678 (14749)	680 (14706) [a]	675 (14815) [a]	681.5 (14674) [c]	680 (14706) [c]	(9)
4 Chl_{D2}	670 (14925)	670 (14925)	670 (14925)	670 (14925)	670 (14925)	(–3)
5 $Pheo_{D1}$	670 (14925)	671 (14903) [a]	671 (14903) [b]	667 (14993) [a]	670 (14925) [a]	(–64)
6 $Pheo_{D2}$	675 (14815)	675 (14815)	675 (14815)	674 (14837)	674.7 (14821)	(–15)
7 $Chlz_{D1}$	670 (14925)	670 (14925)	670 (14925)	670 (14925)	670 (14925)	(4)
8 $Chlz_{D2}$	665 (15038)	665 (15038)	665 (15038)	665 (15038)	665 (15038)	(1)

[a] $\Delta_{inh} = 120\ cm^{-1}$. [b] Chl *a* replacing $Pheo_{D1}$. [c] $\Delta_{inh} = 80\ cm^{-1}$. [d] Calculated based on 3WU2 with APCs for $Q_A^{\bullet}/Q_A$ from Ishikita and Knapp.[12]

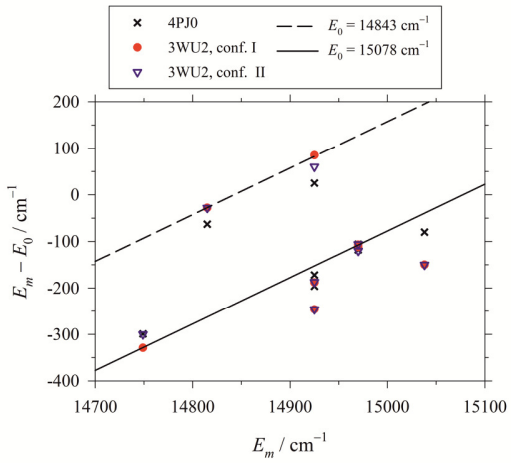

Figure S4: Correlation of computed site energy shifts $E_m - E_0$ with the site energies E_m used to simulate optical spectra of the RC of PSII (Table S7, column I). The lines have slope unity and serve to determine E_0 for Chl (solid line) and Pheo (dashed line). The rms deviation between Table S7, column I and the computed site energies is 34 cm^{-1} for 4PJ0, 52 cm^{-1} for 3WU2, conf. I, and 54 cm^{-1} for 3WU2, conf. II including $Chlz_{D1}/Chlz_{D2}$ as well as 31, 14, and 21 cm^{-1}, respectively, excluding $Chlz_{D1}/Chlz_{D2}$. Using E_0 = 14878 cm^{-1} for the Pheos in 4PJ0, results in a rms deviation of 18 cm^{-1} excluding $Chlz_{D1}/Chlz_{D2}$.

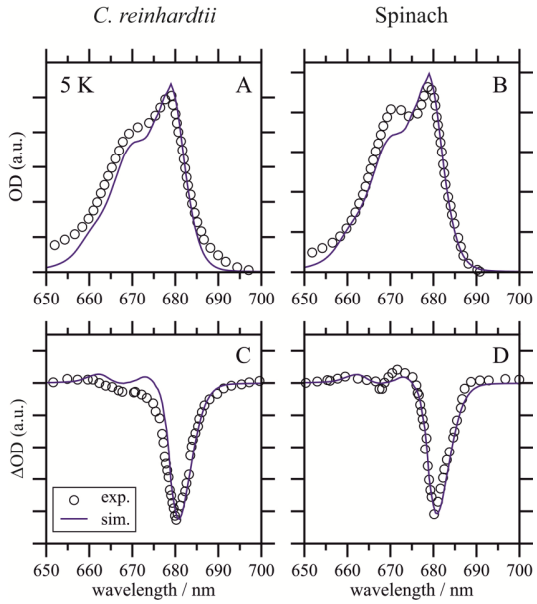

Figure S5: Absorption and transient hole burning spectra of RC preparations from *C. reinhardtii* (left) and spinach (right) as obtained by Chauvet et al.[46] (open symbols). Blue curves are simulations using the structure-based exciton Hamiltonian described in the main text (Table S7, column I). The transient hole burning spectra are simulated as triplet-minus-singlet difference spectra assuming triplet localization on Chl_{D1}.

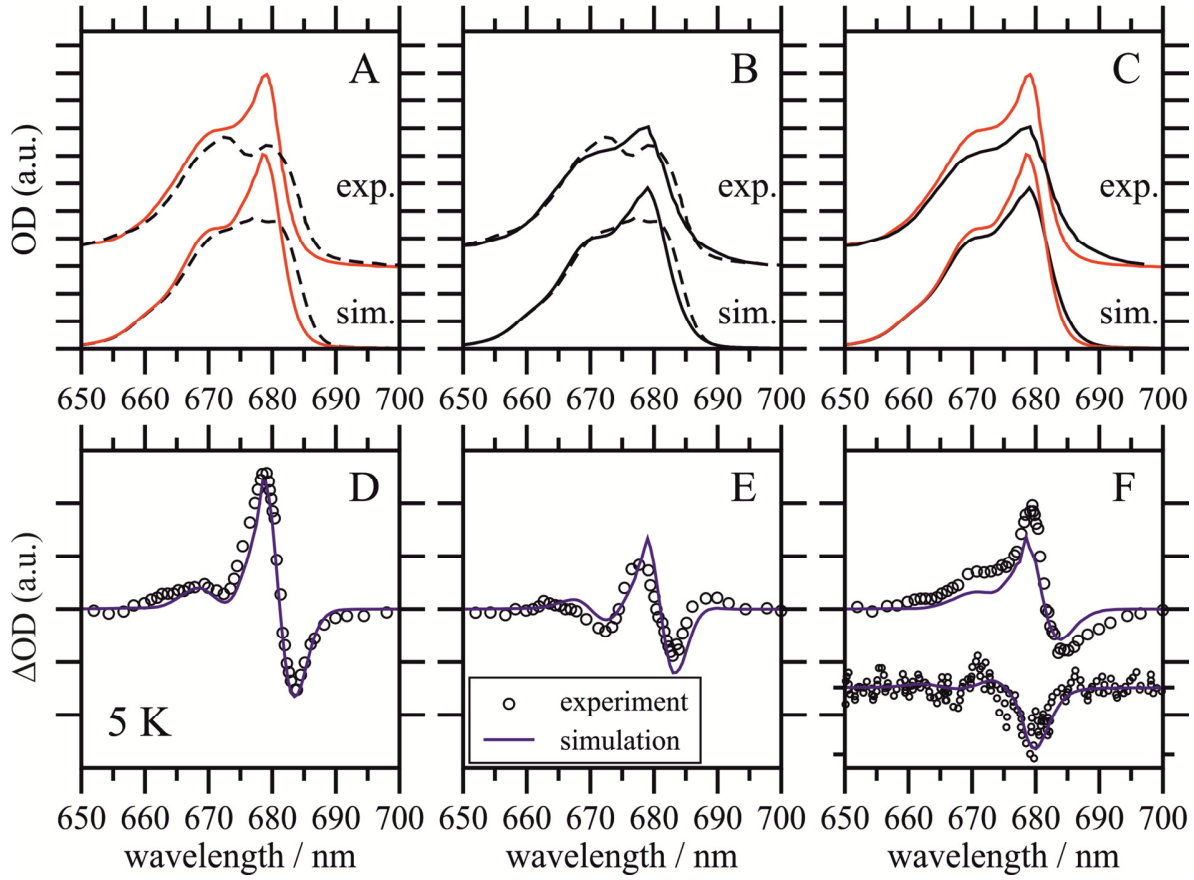

Figure S6: Effects of the mutation LH(D209) in RCs of *C. reinhardtii* (replacement of $Pheo_{D1}$ with Chl *a*). Site energies used in the simulations are compiled in Table S7. Simulations of mutant RCs take into account the increased dipole strength of the pigment in the $Pheo_{D1}$ site as described in S4. A: Absorption spectrum of mutant RCs (red solid curves, site energies in Table S7, column III) compared to so-called "intact" WT RCs (black dashed curves; RCs presumably containing Q_A, site energies in Table S7, column II). Experimental data from Acharya et al.[47] B: Absorption spectrum of "intact" WT RCs (dashed, experimental data from Acharya et al.,[47] site energies in Table S7, column II) compared to presumably Q_A-free WT RCs (solid; experimental data from Chauvet et al.,[46] same as in Figure S5, left, site energies in Table S7, column I). C: The mutant spectrum from A compared to the WT spectrum from B. D: Differences of the spectra in A (mutant minus WT). E: Differences of the spectra in B ("Q_A-free minus "intact"). F: Differences of the spectra in C (mutant minus WT). The inset to F shows a transient hole burning spectrum of the mutant LH(D209) from Acharya et al. together with a simulation of the corresponding triplet-minus-singlet difference spectrum assuming the triplet state to be localized on Chl_{D1} (site energies in Table S7, column III). The latter simulation supports the assignment of a higher site energy to Chl_{D1} in the mutant than in the wild type (cp. Table S7, columns I and III).

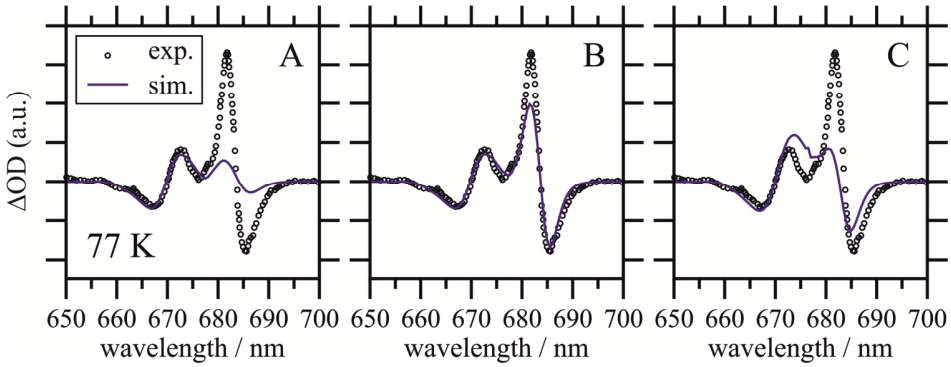

Figure S7: $Q_A^{\bullet}/Q_A$ -difference spectra of PSIIcc from *Synechocystis* PCC 6803. Experimental data from Stewart et al.[48] compared to different simulations. A: Simulation taking into account the electrochromic shifts due to reduction of Q_A computed on the basis of 3WU2 and using the APCs for $Q_A^{\bullet}/Q_A$ from Ishikita and Knapp[12] (Table S7, column VI; for neutral Q_A, column IV). B: Simulation allowing for a larger blueshift of Chl_{D1} due to reduction of Q_A (32 cm^{-1}, Table S7, column V, for neutral Q_A, column IV). C: Same as in B, but with a threshold value of V_c = 50 cm^{-1}, so that exciton delocalization is only allowed between P_{D1} and P_{D2} (cp. Table S4).

S8: Influence of the membrane slab position

Table S8: Site energy shifts $\langle E'_m(\sigma)\rangle_\sigma = E_m - E_0$ in cm^{-1} calculated on the basis of 4PJ0 with different membrane slabs as illustrated in Figure S8 (pH 6.0).

Pigment *m*	Original position [a,b]	Shift 3.5 Å [c]	Shift 6.8 Å [d]	Thickness 20 Å [e]
1 P_{D1}	−118	−120	−122	−120
2 P_{D2}	−106	−110	−107	−106
3 Chl_{D1}	−299	−297	−294	−295
4 Chl_{D2}	−172	−173	−171	−172
5 $Pheo_{D1}$	25	18	9	21
6 $Pheo_{D2}$	−63	−60	−57	−58
7 $Chlz_{D1}$	−196	−195	−196	−200
8 $Chlz_{D2}$	−80	−84	−77	−79

[a] Same as in Table S5. [b] Boundary surfaces determined from atom positions as described in S1 resulting in a slab of thickness 27 Å. [c] Membrane shifted from the original position by 3.5 Å towards the lumenal side. [d] Membrane shifted from the original position by 6.8 Å towards the lumenal side. [e] Membrane of thickness 20 Å with the lower boundary surface shifted by 6.8 Å in the positive *z*-direction with respect to the original membrane.

There is an uncertainty concerning the exact position and thickness of the membrane slab, to which the lower dielectric constant ε_{mem} is assigned. The lipids modeled in the crystal structure can be used as a landmark to define the region of lower polarizability by assuming that the membrane interior is located roughly at the position of the alkyl tails of the lipids. The membrane slab defined on the basis of the position vectors of the nonheme iron and the Mg^{2+} ions of P_{D1} and P_{D2} as described in S1 seems to be slightly offset from the alkyl tail region (Figure S8A). Therefore, a membrane slab shifted by 2 Å towards the lumenal side was used in the

computations based on 3WU2. To test the influence of the precise slab position and thickness on the computed site energies, we also performed calculations based on 4PJ0 with slabs shifted by 3.5 and 6.8 Å towards the lumen as well as a slab of lower thickness (20 Å). As can be seen from Table S8, the influence of these variations is minor, and the asymmetry in site energies is not affected.

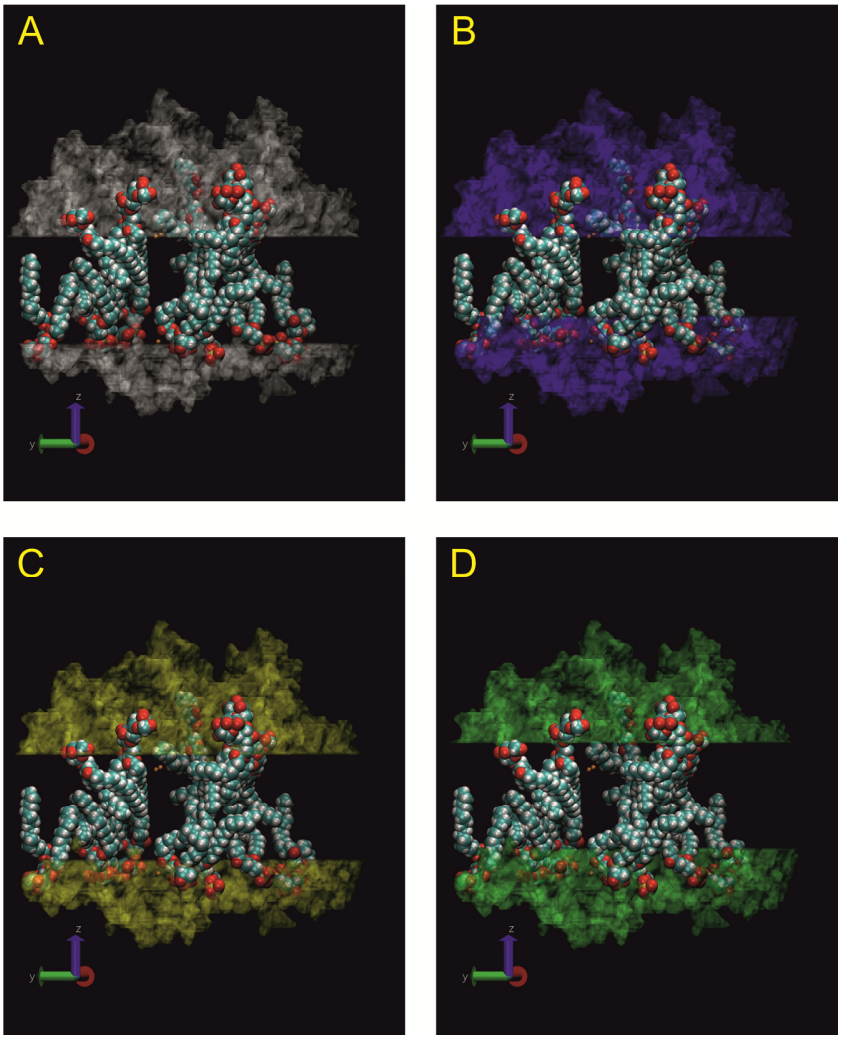

Figure S8: Comparison of different membrane slabs tested. The colored surfaces illustrate the boundary between the protein interior (ε_p, $\tilde{\varepsilon}_p$) and the solvent regions (ε_{solv}) and indirectly also indicate the position of the membrane slab with $\varepsilon_{mem} = 2.0$. As implemented in TAPBS,[16] the coordinate system is rotated such that the membrane normal is parallel to the *z*-axis. Some of the structural lipids contained in the model (cf. Table S2) are shown in vdW-representation. The alkyl tails of these lipids give an indication of the likely position of the membrane interior, which is represented by the region of low dielectric constant. Figures made with VMD.[15]
A: Original membrane of thickness 27 Å defined by atom positions as described in the text (S1). B: Membrane of thickness 20 Å with the lower boundary surface shifted by 6.8 Å in the positive *z*-direction with respect to the original membrane. C: Membrane of thickness 27 Å obtained by shifting the both boundary surfaces by 3.5 Å in the positive *z*-direction. D: Membrane of thickness 27 Å obtained by shifting both boundary surfaces by 6.8 Å in the positive *z*-direction.

S9: Protonation pattern dependent site energy distributions

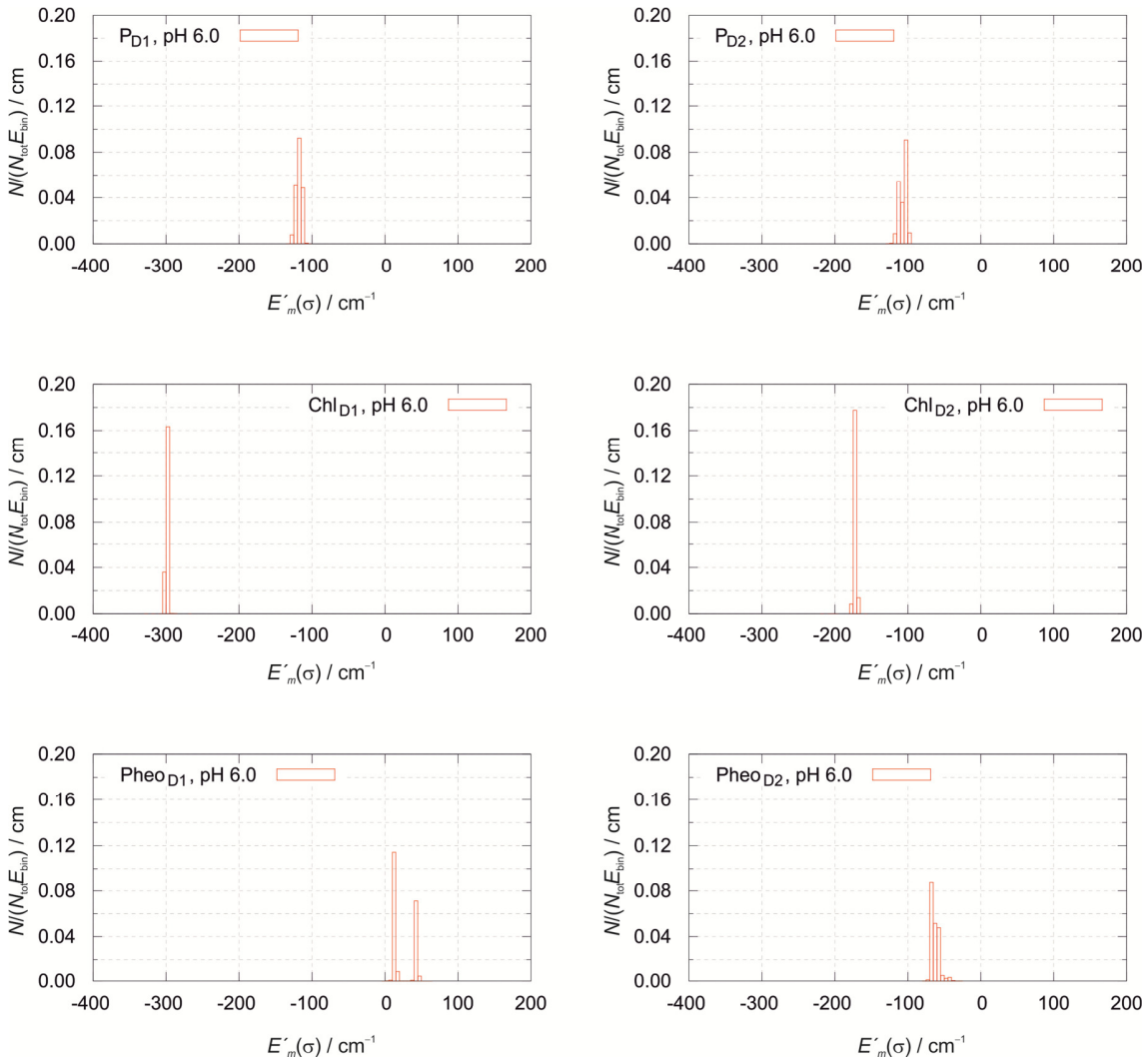

Figure S9: Protonation pattern dependent site energy distributions of the six pigments in the RC of PSII computed on the basis of 4PJ0. The averages of these distributions are the site energy shifts listed in Table S5 (4PJ0 full). These distributions are narrow enough, so that the average site energies can be used in the exciton Hamiltonian (eq. (1) of the main text). Notably, there are two peaks in the distribution of Pheo$_{D1}$, 30 cm^{-1} apart. This splitting is due to Glu D219, which interacts weakly with Pheo$_{D1}$ and has an apparent pK_a value of 5.55, so that it is protonated to 38% at pH 6.0.

S10: Site energies used in previous exciton models

Table S9: Site energies E_m in nm used in previous exciton models of the RC in PSII. Site energies marked in bold are in agreement with the asymmetry found in the present work for the Chl_{D1}/Chl_{D2} and $Pheo_{D1}/Pheo_{D2}$ pairs.

Pigment *m*	Durrant at al., 1995 [51, a]	Prokhorenko, Holzwarth, 2000 [52, b]	Jankowiak et al., 2002 [53, c]	Renger, Marcus, 2002 [54]	Novoderezhkin et al., 2005,[49, d] Model A	B	C	D	2007[50, e]
1 P_{D1}	673	673	673	669	661	662	657	654	658
2 P_{D2}	673	673	673	669	659	648	657	662	659
3 Chl_{D1}	673	671	673	669	662	**663**	**666**	**665**	**667**
4 Chl_{D2}	673	673	673	669	662	**652**	**656**	**661**	**661**
5 $Pheo_{D1}$	673	673	673	669	659	658	663	662	664
6 $Pheo_{D2}$	673	673	668	669	654	654	660	662	664

[a] Original multimer model. [b] From fit of photon echo data. [c] Pentamer model with all excitonic couplings involving $Pheo_{D2}$ set to zero. [d] Simultaneous fit of absorption, LD, CD, steady-state fluorescence, time-resolved absorption, and time-resolved fluorescence. [e] Simultaneous fit of absorption, LD, CD, steady-state fluorescence, triplet-minus-singlet, Stark spectra, and Pheo-modified RCs.

Table S9. Continued.

Pigment *m*	Raszewski et al. 2005[36, a]	Raszewski et al. 2008[37,42, b]	Acharya et al.[47] 2012	Gelzinis et al.[55] 2013	Shibata et al.[38] 2013	Zhang et al.[56, f] 2014	Present work
1 P_{D1}	666	666/670 [c]	665 – 667	654	664	773 / 779	668
2 P_{D2}	666	666	665 – 667	657	668.5	768 / 776	668
3 Chl_{D1}	**678**	**682/679** [c]	678	**666**	**678 / 682** [e]	**782 / 792**	**678**
4 Chl_{D2}	**667**	**667**	– [d]	**661**	**667**	**763 / 780**	**670**
5 $Pheo_{D1}$	**672**	**672**	679 – 681	**664**	**666**	**763 / 766**	**670**
6 $Pheo_{D2}$	**675**	**675**	670	**665**	**675**	**776 / 783**	**675**

[a] Simultaneous fit of absorption, LD, CD, steady-state fluorescence, triplet-minus-singlet, and Pheo-modified RCs. [b] Simulations including time-resolved data. [c] $T \leq 170$ K / $T > 170$ K. [d] Not reported. [e] RC / PSIIcc. [f] From MD simulations at 77 K / 300 K and semi-empirical ZINDO/S computations.

S11: Abbreviations

APC	Atomic partial charge
BCT	Bicarbonate
bRC	Bacterial reaction center
CD	Circular dichroism
CHARMM	Chemistry at HARvard Macromolecular Mechanics (Software)
Chl	Chlorophyll
FMO	Fenna-Matthews-Olson (protein)
ΔOD	Absorption difference
HF-CIS	Hartree-Fock with Configuration Interaction Singles
LD	Linear dichroism
LPBE	Linearized Poisson-Boltzmann equation
MC	Monte Carlo
MD	(Classical) Molecular dynamics
OD	Absorption (optical density)
PBQC	Poisson-Boltzmann/quantum chemical
PDB	Protein data bank (of the Research Collaboratory for Structural Bioinformatics)
Pheo	Pheophytin
PPC	Pigment-protein complex
PSII	Photosystem II
PSIIcc	Photosystem II core complex
RC	Reaction center
TrEsp	Transition charge from electrostatic potential
WOC	Water oxidizing complex

S12: Supporting references

(1) Umena, Y.; Kawakami, K.; Shen, J. R.; Kamiya, N. Crystal Structure of Oxygen-Evolving Photosystem II at a Resolution of 1.9 Å. *Nature* **2011**, *473*, 55-60.

(2) Hellmich, J.; Bommer, M.; Burkhardt, A.; Ibrahim, M.; Kern, J.; Meents, A.; Müh, F.; Dobbek, H.; Zouni, A. Native-Like Photosystem II Superstructure at 2.44 Å Resolution through Detergent Extraction from the Protein Crystal. *Structure* **2014**, *22*, 1607-1615.

(3) Brooks, B. R.; Bruccoleri, R. E.; Olafson, B. D.; States, D. J.; Swaminathan, S.; Karplus, M. CHARMM - a Program for Macromolecular Energy, Minimization, and Dynamics Calculations. *J. Comput. Chem.* **1983**, *4*, 187-217.

(4) Brooks, B. R.; Brooks, C. L.; Mackerell, A. D.; Nilsson, L.; Petrella, R. J.; Roux, B.; Won, Y.; Archontis, G.; Bartels, C.; Boresch, S.; Caflisch, A.; Caves, L.; Cui, Q.; Dinner, A. R.; Feig, M.; Fischer, S.; Gao, J.; Hodoscek, M.; Im, W.; Kuczera, K.; Lazaridis, T.; Ma, J.; Ovchinnikov, V.; Paci, E.; Pastor, R. W.; Post, C. B.; Pu, J. Z.; Schaefer, M.; Tidor, B.; Venable, R. M.; Woodcock, H. L.; Wu, X.; Yang, W.; York, D. M.; Karplus, M. CHARMM: The Biomolecular Simulation Program. *J. Comput. Chem.* **2009**, *30*, 1545-1614.

(5) Nanba, O.; Satoh, K. Isolation of a Photosystem II Reaction Center Consisting of D-1 and D-2 Polypeptides and Cytochrome *b*-559. *Proc. Natl. Acad. Sci. U. S. A.* **1987**, *84*, 109-112.

(6) Ikeuchi, M.; Inoue, Y. A New Photosystem II Reaction Center Component (4.8 kDa Protein) Encoded by Chloroplast Genome. *FEBS Lett.* **1988**, *241*, 99-104.

(7) Webber, A. N.; Packman, L.; Chapman, D. J.; Barber, J.; Gray, J. C. A fifth Chloroplast-Encoded Polypeptide Is Present in the Photosystem II Reaction Centre Complex. *FEBS Lett.* **1989**, *242*, 259-262.

(8) Ikeuchi, M.; Koike, H.; Inoue, Y. Identification of *psb*I and *psb*L Gene Products in Cyanobacterial Photosystem II Reaction Center Preparation. *FEBS Lett.* **1989**, *251*, 155-160.

(9) Müh, F.; Zouni, A. Cytochrome b_{559} in Phoptosystem II In *Cytochrome Complexes: Evolution, Structures, Energy Transduction, and Signaling*; Cramer, W. A., Kallas, T., Eds.; Springer: Dordrecht, 2016; pp 143-175.

(10) MacKerell, A. D.; Bashford, D.; Bellott, M.; Dunbrack, R. L.; Evanseck, J. D.; Field, M. J.; Fischer, S.; Gao, J.; Guo, H.; Ha, S.; Joseph-McCarthy, D.; Kuchnir, L.; Kuczera, K.; Lau, F. T. K.; Mattos, C.; Michnick, S.; Ngo, T.; Nguyen, D. T.; Prodhom, B.; Reiher, W. E.; Roux, B.; Schlenkrich, M.; Smith, J. C.; Stote, R.; Straub, J.; Watanabe, M.; Wiorkiewicz-Kuczera, J.; Yin, D.; Karplus, M. All-Atom Empirical Potential for Molecular Modeling and Dynamics Studies of Proteins. *J. Phys. Chem. B* **1998**, *102*, 3586-3616.

(11) Ishikita, H.; Knapp, E. W. Redox Potential of Quinones in Both Electron Transfer Branches of Photosystem I. *J. Biol. Chem.* **2003**, *278*, 52002-52011.

(12) Ishikita, H.; Knapp, E. W. Redox Potentials of Chlorophylls and β-Carotene in the Antenna Complexes of Photosystem II. *J. Am. Chem. Soc.* **2005**, *127*, 1963-1968.

(13) Ishikita, H.; Loll, B.; Biesiadka, J.; Kern, J.; Irrgang, K. D.; Zouni, A.; Saenger, W.; Knapp, E. W. Function of Two β-Carotenes Near the D1 and D2 Proteins in Photosystem II Dimers. *Biochim Biophys Acta* **2007**, *1767*, 79-87.

(14) Cannon, W. R.; Pettitt, B. M.; McCammon, J. A. Sulfate Anion in Water - Model Structural, Thermodynamic, and Dynamic Properties. *J. Phys. Chem. B* **1994**, *98*, 6225-6230.

(15) Humphrey, W.; Dalke, A.; Schulten, K. VMD: Visual Molecular Dynamics. *J. Mol. Graphics* **1996**, *14*, 33-38.

(16) Kieseritzky, G.; Knapp, E. W. Optimizing pK_A Computation in Proteins with pH Adapted Conformations. *Proteins* **2008**, *71*, 1335-1348.

(17) Baker, N. A.; Sept, D.; Joseph, S.; Holst, M. J.; McCammon, J. A. Electrostatics of Nanosystems: Application to Microtubules and the Ribosome. *Proc. Natl. Acad. Sci. U. S. A.* **2001**, *98*, 10037-10041.

(18) Müh, F.; Madjet, M. E.; Adolphs, J.; Abdurahman, A.; Rabenstein, B.; Ishikita, H.; Knapp, E. W.; Renger, T. α-Helices Direct Excitation Energy Flow in the Fenna-Matthews-Olson Protein. *Proc. Natl. Acad. Sci. U. S. A.* **2007**, *104*, 16862-16867.

(19) Renger, T.; Müh, F. Understanding Photosynthetic Light-Harvesting: A Bottom Up Theoretical Approach. *Phys. Chem. Chem. Phys.* **2013**, *15*, 3348-3371.

(20) Shao, Y.; Molnar, L. F.; Jung, Y.; Kussmann, J.; Ochsenfeld, C.; Brown, S. T.; Gilbert, A. T. B.; Slipchenko, L. V.; Levchenko, S. V.; O'Neill, D. P.; DiStasio, R. A.; Lochan, R. C.; Wang, T.; Beran, G. J. O.; Besley, N. A.; Herbert, J. M.; Lin, C. Y.; Van Voorhis, T.; Chien, S. H.; Sodt, A.; Steele, R. P.; Rassolov, V. A.; Maslen, P. E.; Korambath, P. P.; Adamson, R. D.; Austin, B.; Baker, J.; Byrd, E. F. C.; Dachsel, H.; Doerksen, R. J.; Dreuw, A.; Dunietz, B. D.; Dutoi, A. D.; Furlani, T. R.; Gwaltney, S. R.; Heyden, A.; Hirata, S.; Hsu, C. P.; Kedziora, G.; Khalliulin, R. Z.; Klunzinger, P.; Lee, A. M.; Lee, M. S.; Liang, W.; Lotan, I.; Nair, N.; Peters, B.; Proynov, E. I.; Pieniazek, P. A.; Rhee, Y. M.; Ritchie, J.; Rosta, E.; Sherrill, C. D.; Simmonett, A. C.; Subotnik, J. E.; Woodcock, H. L.; Zhang, W.; Bell, A. T.; Chakraborty, A. K.; Chipman, D. M.; Keil, F. J.; Warshel, A.; Hehre, W. J.; Schaefer, H. F.; Kong, J.; Krylov, A. I.; Gill, P. M. W.; Head-Gordon, M. Advances in Methods and Algorithms in a Modern Quantum Chemistry Program Package. *Phys. Chem. Chem. Phys.* **2006**, *8*, 3172-3191.

(21) Sigfridsson, E.; Ryde, U. Comparison of Methods for Deriving Atomic Charges from the Electrostatic Potential and Moments. *J. Comput. Chem.* **1998**, *19*, 377-395.

(22) Madjet, M. E.; Abdurahman, A.; Renger, T. Intermolecular Coulomb Couplings from Ab Initio Electrostatic Potentials: Application to Optical Transitions of Strongly Coupled Pigments in Photosynthetic Antennae and Reaction Centers. *J. Phys. Chem. B* **2006**, *110*, 17268-17281.

(23) Krawczyk, S. Electrochromism of Chlorophyll *a* Monomer and Special Pair Dimer. *Biochim. Biophys. Acta* **1991**, *1056*, 64-70.

(24) van Dijk, B.; Hoff, A. J.; Shkuropatov, A. Y. Electrooptical properties of Different Redox States of Native and Modified Reaction Centers of *Rhodobacter sphaeroides*. *J. Phys. Chem. B* **1998**, *102*, 8091-8099.

(25) Ullrich, C. A.; Yang, Z. H. A Brief Compendium of Time-Dependent Density Functional Theory. *Braz. J. Phys.* **2014**, *44*, 154-188.

(26) Madjet, M. E.; Müh, F.; Renger, T. Deciphering the Influence of Short-Range Electronic Couplings on Optical Properties of Molecular Dimers: Application to "Special Pairs" in Photosynthesis. *J. Phys. Chem. B* **2009**, *113*, 12603-12614.

(27) Hirata, S.; Head-Gordon, M. Time-Dependent Density Functional Theory within the Tamm-Dancoff Approximation. *Chem. Phys. Lett.* **1999**, *314*, 291-299.

(28) Yanai, T.; Tew, D. P.; Handy, N. C. A New Hybrid Exchange-Correlation Functional using the Coulomb-Attenuating Method (CAM-B3LYP). *Chem. Phys. Lett.* **2004**, *393*, 51-57.

(29) Ullmann, G. M.; Knapp, E. W. Electrostatic Models for Computing Protonation and Redox Equilibria in Proteins. *Eur. Biophys. J.* **1999**, *28*, 533-551.

(30) Bashford, D. Macroscopic Electrostatic Models for Protonation States in Proteins. *Front. Biosci.* **2004**, *9*, 1082-1099.

(31) Simonson, T.; Perahia, D. Microscopic Dielectric Properties of Cytochrome *c* from Molecular Dynamics Simulations in Aqueous Solution. *J. Am. Chem. Soc.* **1995**, *117*, 7987-8000.

(32) Simonson, T.; Brooks, C. L. Charge Screening and the Dielectric Constant of Proteins: Insights from Molecular Dynamics. *J. Am. Chem. Soc.* **1996**, *118*, 8452-8458.

(33) Metropolis, N.; Rosenbluth, A. W.; Rosenbluth, M. N.; Teller, A. H.; Teller, E. Equation of State Calculations by Fast Computing Machines. *J. Chem. Phys.* **1953**, *21*, 1087-1092.

(34) Rabenstein, B.; Knapp, E. W. Calculated pH-Dependent Population and Protonation of Carbon-Monoxy-Myoglobin Conformers. *Biophys. J.* **2001**, *80*, 1141-1150.

(35) Renger, T.; Marcus, R. A. On the Relation of Protein Dynamics and Exciton Relaxation in Pigment-Protein Complexes: An Estimation of the Spectral Density and a Theory for the Calculation of Optical Spectra. *J. Chem. Phys.* **2002**, *116*, 9997-10019.

(36) Raszewski, G.; Saenger, W.; Renger, T. Theory of Optical Spectra of Photosystem II Reaction Centers: Location of the Triplet State and the Identity of the Primary Electron Donor. *Biophys. J.* **2005**, *88*, 986-998.

(37) Raszewski, G.; Diner, B. A.; Schlodder, E.; Renger, T. Spectroscopic Properties of Reaction Center Pigments in Photosystem II Core Complexes: Revision of the Multimer Model. *Biophys. J.* **2008**, *95*, 105-119.

(38) Shibata, Y.; Nishi, S.; Kawakami, K.; Shen, J. R.; Renger, T. Photosystem II Does Not Possess a Simple Excitation Energy Funnel: Time-Resolved Fluorescence Spectroscopy Meets Theory. *J. Am. Chem. Soc.* **2013**, *135*, 6903-6914.

(39) Adolphs, J.; Müh, F.; Madjet, M. E.; Renger, T. Calculation of Pigment Transition Energies in the FMO Protein. *Photosynth. Res.* **2008**, *95*, 197-209.

(40) Renger, T.; Müh, F. Theory of Excitonic Couplings in Dielectric Media. Foundation of Poisson-TrEsp Method and Application to Photosystem I Trimers. *Photosynth. Res.* **2012**, *111*, 47-52.

(41) Renger, T.; Madjet, M. E.; Schmidt am Busch, M.; Adolphs, J.; Müh, F. Structure-Based Modeling of Energy Transfer in Photosynthesis. *Photosynth. Res.* **2013**, *116*, 367-388.

(42) Raszewski, G.; Renger, T. Light Harvesting in Photosystem II Core Complexes Is Limited by the Transfer to the Trap: Can the Core Complex Turn into a Photoprotective Mode? *J. Am. Chem. Soc.* **2008**, *130*, 4431-4446.

(43) Knox, R. S.; Spring, B. Q. Dipole Strengths in the Chlorophylls. *Photochem. Photobiol.* **2003**, *77*, 497-501.

(44) Renger, T.; Madjet, M. E.; Müh, F.; Trostmann, I.; Schmitt, F. J.; Theiss, C.; Paulsen, H.; Eichler, H. J.; Knorr, A.; Renger, G. ThermallyActivated Superradiance and Intersystem Crossing in the Water-Soluble Chlorophyll Binding Protein. *J. Phys. Chem. B* **2009**, *113*, 9948-9957.

(45) Houssier, C.; Sauer, K. Circular Dichroism and Magnetic Circular Dichroism of the Chlorophyll and Protochlorophyll Pigments. *J. Am. Chem. Soc.* **1970**, *92*, 779-791.

(46) Chauvet, A.; Jankowiak, R.; Kell, A.; Picorel, R.; Savikhin, S. Does the Singlet Minus Triplet Spectrum with Major Photobleaching Band Near 680-682 nm Represent an Intact Reaction Center of Photosystem II? *J. Phys. Chem. B* **2015**, *119*, 448-455.

(47) Acharya, K.; Neupane, B.; Zazubovich, V.; Sayre, R. T.; Picorel, R.; Seibert, M.; Jankowiak, R. Site Energies of Active and Inactive Pheophytins in the Reaction Center of Photosystem II from *Chlamydomonas reinhardtii*. *J. Phys. Chem. B* **2012**, *116*, 3890-3899.

(48) Stewart, D. H.; Nixon, P. J.; Diner, B. A.; Brudvig, G. W. Assignment of the Q_y Absorbance Bands of Photosystem II Chromophores by Low-Temperature Optical Spectroscopy of Wild-Type and Mutant Reaction Centers. *Biochemistry* **2000**, *39*, 14583-14594.

(49) Novoderezhkin, V. I.; Andrizhiyevskaya, E. G.; Dekker, J. P.; van Grondelle, R. Pathways and Timescales of Primary Charge Separation in the Photosystem II Reaction Center As

Revealed by a Simultaneous Fit of Time-Resolved Fluorescence and Transient Absorption. *Biophys. J.* **2005**, *89*, 1464-1481.

(50) Novoderezhkin, V. I.; Dekker, J. P.; van Grondelle, R. Mixing of Exciton and Charge-Transfer States in Photosystem II Reaction Centers: Modeling of Stark Spectra with Modified Redfield Theory. *Biophys. J.* **2007**, *93*, 1293-1311.

(51) Durrant, J. R.; Klug, D. R.; Kwa, S. L. S.; van Grondelle, R.; Porter, G.; Dekker, J. P. A Multimer Model for P680, the Primary Electron Donor of Photosystem II. *Proc. Natl. Acad. Sci. U. S. A.* **1995**, *92*, 4798-4802.

(52) Prokhorenko, V. I.; Holzwarth, A. R. Primary Processes and Structure of the Photosystem II Reaction Center: A Photon Echo Study. *J. Phys. Chem. B* **2000**, *104*, 11563-11578.

(53) Jankowiak, R.; Hayes, J. M.; Small, G. J. An Excitonic Pentamer Model for the Core Q_y States of the Isolated Photosystem II Reaction Center. *J. Phys. Chem. B* **2002**, *106*, 8803-8814.

(54) Renger, T.; Marcus, R. A. Photophysical Properties of PS-2 Reaction Centers and a Discrepancy in Exciton Relaxation Times. *J. Phys. Chem. B* **2002**, *106*, 1809-1819.

(55) Gelzinis, A.; Valkunas, L.; Fuller, F. D.; Ogilvie, J. P.; Mukamel, S.; Abramavicius, D. Tight-Binding Model of the Photosystem II Reaction Center: Application to Two-Dimensional Electronic Spectroscopy. *New J. Phys.* **2013**, *15*.

(56) Zhang, L.; Silva, D. A.; Zhang, H. D.; Yue, A.; Yan, Y. J.; Huang, X. H. Dynamic Protein Conformations Preferentially Drive Energy Transfer Along the Active Chain of the Photosystem II Reaction Centre. *Nat. Commun.* **2014**, *5*, 4170.